Photovoltaic application of the multiferroic Bi_2FeCrO_6 double perovskite

C. Tablero
Instituto de Energía Solar, E.T.S.I. de Telecomunicación,
Universidad Politécnica de Madrid,
Ciudad Universitaria s/n, 28040 Madrid, SPAIN.
e-mail: ctablero@etsit.upm.es

Abstract

Bi_2FeCrO_6 double-perovskite is a multiferroic semiconductor with ferromagnetic and ferroelectric properties that allows a variety of applications including optoelectronic and photovoltaic applications. An analysis focusing on the potential for solar cells is carried out starting from first-principles. The optoelectronic properties are characterized by two threshold spin gaps. Using the absorption coefficients from first-principles, the efficiencies are evaluated for several sunlight spectra, light concentrations and the usual radiative and ferroelectric photovoltaic mechanisms. The results indicate a huge potential as an absorber of the solar spectrum.

Keywords: photovoltaic effects, Ferroelectric, Semiconductors, Efficiency, Multi-gap

1. Introduction.

Multiferroic materials have potential applications in spintronics, optoelectronics and recently in photovoltaics [1,2]. The ferroelectricity and ferromagnetism can hardly coexist in the same material. Therefore these multiferroic materials are very rare. For ferroelectricity and magnetism to coexist, the atoms responsible for the ferroelectric (FE) polarization should be different from those that carry the magnetic moment (i.e., magnetization).

On the other hand, because of the wide bandgap of FE materials, the sunlight absorption is poor making them unsuitable for photovoltaic (PV) applications. Thus, to

obtain solar cells with greater efficiency, it is necessary to reduce the bandgap without affecting the FE properties. Because of its relatively low bandgap (~2.6 eV) compared with others FE materials $BiFeO_3$ (BFO) has been largely researched for PV applications. However, their bandgap is larger than the optimum value for obtaining the maximum efficiency (~41 % at Eg=1.1 eV and at the highest sunlight concentration = 46200 sun, where 1 sun = 1 $kW/m^{2,}$ and ~31 % at Eg=1.3 eV for 1 sun) [3-6].

Therefore, additional chemical modification of the transition metal in the perovskite octahedra sites of the BFO structure is necessary to allow the bandgap to be lowered without affecting ferroelectricity. Additionally, the stereochemical activity of Bi can be exploited to induce structural distortions with the goal of forming multiferroic materials, which can be done using double perovskites $A_2M'MX_6$, a group of materials derived from the perovskite structure (AMX_3). In the case of the oxide (X=O), the M and M' cations are octahedrally coordinated by oxygen. The introduction of A ions lead indirectly to a structural modification of the MO_6 and $M'O_6$ octahedral. This provides a mechanism for modifying the electronic structure through the use of A ions.

Multiferroic Bi_2FeCrO_6 (BFCO), with a double perovskite structure, and with FE and magnetic properties, was predicted theoretically from first-principles calculations [7] and later synthesized experimentally [8,9]. In BFCO, ferroelectricity is due to the $6s^2$ lone pair on Bi^{3+} ions at A sites, a well-established mechanism in other multiferroics, such as $BiMnO_3$ [10] and BFO, [11] while magnetism is introduced via ferromagnetic behavior. The coupling between neighboring chromium (Cr) and iron (Fe) magnetic moments is robustly antiferromagnetic, and the difference between their magnetizations yields a net magnetization for BFCO.

BFCO has been studied for applications in solar energy conversion because of their efficient FE polarization and above-bandgap generated photovoltages [2], which in principle can lead to high energy conversion efficiencies beyond the maximum value reported in traditional solar cells. However, the efficiencies reported so far are still low. After polarization was positively oriented to maximize the FE driving force a PV power conversion efficiency of about 8.1 % under AM1.5G illumination spectra [12] was achieved [9], and with short circuit current density Jsc = 20.6 mA cm^{-2} and open circuit voltage Voc = 0.84 eV.

The additional PV effect in FE semiconductors (FE-PV) is different from the usual radiative PV effect. The polarization electric field is the driving force behind the photocurrent in FE-PV devices. In addition the open-circuit voltage can be larger than the bandgap of the FE materials (anomalous effect). In contrast to the huge photovoltage output, the photocurrents of the FE-PV device are quite low, usually in the order of $nA.cm^{-2}$ [13,14]. This is the reason for the low solar energy conversion efficiency.

Despite the promising properties, the real potential of semiconducting FE perovskites in PV applications is far from being fulfilled. The main experimental and theoretical research activities focus on exploring the origin of the observed FE-PV properties. However, despite experimental and theoretical research activities, there is little analysis focusing on the coexistence of the usual radiative-PV and FE-PV effects in FE semiconductors. Further applications of these materials require a detailed understanding of their electronic and optical properties. First-principles calculations are an important and powerful complementary tool, allowing these basic properties, which are hardly accessible by experiments, to be obtained and quantified. Therefore we examine the electronic and optical properties using first-principles techniques. From these results the possible application in solar energy conversion is analyzed.

2. Methodology

In order to obtain the electronic properties, we use first principles within the density functional formalism [15,16] but with a further extension including an orbital-dependent, one-electron potential (DFT+U method) [17] to account explicitly for the Coulomb repulsions not dealt with adequately in standard DFT approaches. The DFT+U results depend on the U value, on the orbital subspace in which U is applied, on the orbital occupation numbers, and on the implementation chosen [17-21]. In this work we use the DFT+U formalism described in references [18,19] with the generalized gradient approximation from Perdew, Burke and Ernzerhof [22] for the exchange-correlation potential, i.e. GGA+U. The pseudopotentials adopted are standard Troullier–Martins [23] expressed in the Kleinman–Bylander [24] factorized form. A numerically localized pseudoatomic orbital basis set [25] is used for the valence wave functions. The structure with *R*3 symmetry (space group 146), periodic boundary conditions, spin polarization, double-zeta with polarization localized basis sets, U=10 eV, and 256 special *k* points in the irreducible Brillouin zone have been used in all results presented in this work.

The optical properties have been obtained on the independent-particle approximation from the complex dielectric function

$$e_2(E) \sim \frac{1}{E^2} \sum_{\mu} \sum_{\lambda > \mu} \int d\vec{k} \; [f_{\mu,\vec{k}} - f_{\lambda,\vec{k}}] |p_{\mu\lambda}|^2 \, \delta(E_{\lambda,\vec{k}} - E_{\mu,\vec{k}} - E)$$

using the Kramers-Kronig relationships. Here $E_{\mu,\vec{k}}$ and $f_{\mu,\vec{k}}$ are the single-particle energies and occupations of the μ band at $\vec{k}$ points in the Brillouin zone, and $p_{\mu\lambda}$ are the momentum (p=i(m/ħ)[H,r]) matrix elements between the μ and λ bands at $\vec{k}$ points.

3. Results and Discussion.

3.1 Electronic properties

The BFCO has rhombohedral structure with *R*3 symmetry (space group 146) with a lattice parameter a=5.47 Å and an angle α=60.09° [7]. The ground-state structure is ferrimagnetic with a magnetization of 2 μ_B per formula unit [7-9]. The coupling between neighboring chromium (Cr) and iron (Fe) magnetic moments is antiferromagnetic, equivalent to the so-called *G*-type antiferromagnetic ordering, in which all spins within the same (111) plane are ferromagnetically aligned, with an antiparallel alignment of spins in adjacent (111) planes. The energy bandgap experimental is 1.4 eV and direct.

From our results the energy gaps of the ferrimagnetic BFCO for the spin up and down channels are $E_g = E_g^{(+)}$=1.22 eV and $E_g^{(-)}$=2.39 eV respectively. The energy gap E_g compares well with the experimental results (1.4 eV [9]), and with previous theoretical results: 0.84 eV [26], 1 eV [7] and 1.48 eV [27]. The experimental optical absorption spectra of BFCO films [9] suggest the presence of two threshold gaps because of the peak structures between 1.5-2.7 eV, and a minimum of $(\alpha E)^2$ between 2.1-2.4 eV. It is in accordance with the two energy gaps for the two spins and with the calculated absorption coefficient, which has been split for each spin component in panels (a) and (b) in Figure 1.

In the BFCO double perovskite, the M (M=Fe and Cr) atoms are approximately octahedrally coordinated by oxygen [1,2]. Therefore, the geometry around the M sites is a distorted octahedral. The *d*(M) states are split roughly into d_e(M) (d_{z^2} and $d_{x^2-y^2}$) and d_t(M) (d_{xy}, d_{xz}, and d_{yz}) states respectively. The *t* symmetry crystalline wavefunctions are formed mainly through the combination of the d_t(M) states with the p_t(O) states of the nearest oxygen atoms. The analyses of states reveal that the states of the VB edge are

derived mainly from p(O)+s(Bi), and with a lower proportion from p(Bi) states. The CB edge states with spin-up are derived mainly from the combination of the d(Fe)+p(O)+d(Cr) states, whereas the spin-down CB edge states are derived from the p(Bi)+p(O) states.

3.2 Absorption coefficient

The experimental optical absorption spectra of BFCO films [9] suggest the presence of two threshold gaps because of the peak structures between 1.5-2.7 eV, and a minimum of $(\alpha E)^2$ between 2.1-2.4 eV, which is in accordance with our optical absorption results in Figure 1. In this figure the absorption coefficient has been split for each spin component in panels (a) and (b).

In order to evaluate the contributions to the absorption coefficient, we have split α into angular momentum contributions as: $\alpha = \sum_A \sum_B \sum_{l_A \in A} \sum_{l_B \in B} \alpha_{l_A l_B}^{AB}$ + (terms involving three and four different non-equivalent species), where $\alpha_{l_A l_B}^{AB}$ indicates the contribution from the transition between the l_A shell-states (in A) and the l_B shell-states (in B). The more important $\alpha_{l_A l_B}^{AB}$ contributions to the absorption coefficient are represented in Figure 2. Between $E_g^{(+)} \le E \le E_g^{(-)}$ the main contribution is from α_{sp}^{OO}, α_{ss}^{BiO}, and α_{pd}^{OFe}. For energies above $E_g^{(-)}$ the two spin components are similar, with $\alpha_{sp}^{BiBi} >> \alpha_{sp}^{OO}$, and α_{ss}^{BiO}. The other transitions, not shown in the Figure, make a very low contribution. As usual we use the notation *s, p, d*, etc for *l*=0, 1, 2, etc.

3.3 Efficiencies

Using the energy gap as a criterion, and considering only the traditional radiative (R-PV) effect, the efficiency of the BFCO single-gap semiconductor should be high

since the energy gap is closer to the optimum for a single gap solar cell (~ 41% at E_g ~ 1.1 eV, and at the highest sunlight concentration f_C =46200 sun, where 1 sun=1 KW/m^2) [3-6]. The efficiencies depend on the spectrum used and the spectral intensity modeled with the concentration factor f_C.

In order to estimate the potentiality of BFCO as a solar-cell device, we have obtained the maximum efficiency. We have assumed the usual approximations [3-6], except that the cell absorbs all incident photons above the bandgap. It implicitly implies that the absorption coefficients are a step function (0 for E < Eg and a constant for E ≥ Eg, where Eg is the energy semiconductor bandgap). With this approximation the efficiency is determined mainly by the band-gap energy. However, the absorption depends on the absorption coefficient. For this reason we have used the absorption coefficients obtained from first principles instead of step functions. Because of this, the efficiencies depend additionally on the thickness *w* of the device. This fact is relevant in nano-electronic devices. In Figure 3 the efficiencies using the spectrum of a 5760 K blackbody reduced by the factor 46200 (BB), and the AM1.5G illumination spectra [12] are shown, both with and without light concentration. In addition to the overall efficiency, the efficiencies for each spin channel are also shown. From the figure, solar cell devices based on BFCO, a few microns thick, could reach efficiencies close to the maximum efficiencies (~31 % at Eg ~ 1.3 eV for the BB spectrum, and ~33 % at Eg ~ 1.4 eV for the AM1.5G spectrum) [3-4]. It shows the huge potentiality of these materials as solar cell absorbers of the solar spectrum. When non-ideal conditions are considered the efficiencies are lower. But these maximum efficiencies enable an evaluation whether the material has the appropriate properties for absorbing solar radiation: if the maximum efficiencies are small the absorbent material is not suitable for solar cells.

So far we have only considered the R-PV effect. Multiferroic films, like the BFCO, are being studied for applications in solar energy conversion because of their FE polarization-driven carrier separation and above-bandgap generated photovoltages because of the bulk PV effect (FE-PV) [13,14].

Under AM1.5G illumination spectra [12] without light concentration (with f_C = 1 sun, where 1 sun = 1 kW/m^2) and after polarization was positively oriented to maximize the FE driving force of the photocharges generated during the measurements, a conversion efficiency of 8.1% (short-circuit current Jsc= 20.6 mA.cm^{-2}, open-circuit voltage Voc = 0.84 eV and fill-factor FF = 0.46) for Bi_2FeCrO_6 thin-film solar cells in a multilayer configuration has been reported [9]. Switching the FE polarization reverses the sign of the Voc and Jsc of the device, indicating that the FE-PV effect is dominant.

According to the results in the literature, a power conversion efficiency as high as 20% is expected based on optimized perovskite-based solid-state solar cells with a bandgap ~ 1.5 eV [28]. This limit is obtained assuming [29] that a maximum current density of 28 mA.cm^{-2} is possible by converting photons in the range of 280−820 nm (4.428-1.51 eV) into electrons, considering 20% light reflection (decreasing in current from 28 mA.cm^{-2} to ~22 mA.cm^{-2}) and a photovoltage of 1.1 V [28].

With the R-PV effect, the maximum efficiency, and the related voltages and currents, under AM1.5G illumination spectra for a bandgap Eg=1.5 eV are ~32 %, ~1.13 V and ~28 mA.cm^{-2} respectively. This limit is closer to maximum (~33 % at an Eg~ 1.4 eV, V=1.05 V and J=32 mA.cm^{-2}). When there is reflection ($0<R\leq1$), the currents and efficiencies are approximately $J(R)=(1-R)J(0)$ and $\eta(R)=(1-R)\eta(0)$. Therefore, considering 20% light reflection (R=0.2), the efficiency and current are 25 % and 22 mA.cm^{-2} respectively. It indicates that the conversion efficiency of the R-PV and FE-PV effects considered independently are similar.

If the two mechanism coexist, the maximum voltage will be limited by Eg=1.5 eV. As the maximum current remains the same (28 $mA.cm^{-2}$) the efficiency will increase to ~ 43 % with R=0 (35 % with R=0.2). This limit corresponds to suppressing the emitted current completely. This current is due to that part of the absorbed photons, which produce a current J_a, are emitted from the solar cell because of the radiative recombination of the R-PV effect. Therefore the current J_e associated with these emitted photons do not contribute to the total current J, i.e. $J= J_a – J_e$. The evolution of the maximum efficiencies and voltages at a Eg=1.5 eV with the decrease of the emitted current: $J(\beta)= J_a – (1-\beta)J_e$, where β represents the degree of removal of J_e is shown in Figure 4. When β increase from 0 (without removing J_e) to 1 (the total elimination of J_e) there is an almost perfect correlation between the maximum efficiencies and the voltages. It indicates that the increase in efficiency is mainly due to the increase in the output voltage.

Additionally, with the R-PV effect, the efficiency can be increased using multi-gap solar cells, with optimum gaps larger than for single-gap solar cells [3-6]. The multi-gap semiconductors contain intermediate bands (IB) between the traditional valence band (VB) and conduction band (CB). So the photon with lower energy than single-gap energy (between the VB and CB) can be exploited (between VB-IB and IB-CB transitions) for generating additional current and increasing the efficiency.

In order to estimate the potentiality of these materials as multi-gap solar-cell devices, we have obtained the maximum efficiency using a generalized multi-gap model [3-6]. From the results, the limiting BFCO efficiencies under AM1.5G illumination spectra with R=0 are η(3b)=41.21 % (J=45 $mA.cm^{-2}$, V=0.91 V), and η(4b)=40.47 % (J=43 $mA.cm^{-2}$, V=0.94 V) from double- to triple–gap solar cells. In all cases these values exceed the limits of single-gap solar cell η(2b)=32.04 (J=28 $mA.cm^{-2}$, V=1.13

V) and are closer to the limit ~ 43 % when the two mechanism, R-PV and FE-FV, coexist.

4. Conclusions.

The potential of multiferroic (ferrimagnetic+FE) BFCO double-perovskite for PV applications has been evaluated. To achieve this objective we have obtained the electronic and optical properties using GGA+U first-principles density-functional theory. The two different gaps for the spin-up and spin-down components are in accordance with the experimental optical absorption spectra and their interpretation with two threshold gaps. With a generalized radiative multi-gap model that makes use of the absorption coefficients from first-principles, the maximum efficiencies are evaluated for several spectra and light concentrations. Efficiencies close to the maximum could be reached with these materials just a few microns thick. In addition to the traditional R-PV effect, the FE-PV effect has also been considered. With the coexistence of the two PV effects the application to solar cells improves slightly. These high expectations would be even higher if intermediate bands could be inserted into BFCO bandgap resulting in a multi-gap semiconductor.

Acknowledgments

This work has been supported by the National Spanish project MADRID-PV (S2013/MAE-2780).

References

[1] S.Y. Yang, L.W. Martin, S.J. Byrnes, T.E. Conry, S.R. Basu, D. Paran, L. Reichertz, J. Ihlefeld, C. Adamo, A. Melville, Y.H. Chu, C.H. Yang, J.L. Musfeldt, D.G. Schlom, J.W. Ager, R. Ramesh, Photovoltaic effects in $BiFeO_3$. Appl. Phys. Lett. 95 (2009) 062909.

[2] S. Y. Yang, J. Seidel, S. J. Byrnes, P. Shafer, C.-H. Yang, M. D. Rossell, P. Yu, Y.-H. Chu, J. F. Scott, J.W. Ager, L. W. Martin and R. Ramesh, Above-bandgap voltages from ferroelectric photovoltaic devices, *Nature Nanotechnology* 5 (2010) 143 – 147.

[3] A. Luque and A. Martí, Theoretical Limits of Photovoltaic Conversion, in Handbook of Photovoltaic Science and Engineering Edited by A. Luque and S. Hegedus, John Wiley & Sons Ltd (2003).

[4] P. Würfel, Physics of Solar Cells. From Principles to New Concepts, 2005 WILEY-VCH Verlag GmbH & Co, KGaA.

[5] M.A. Green, Third Generation Photovoltaics. Advanced Solar Energy Conversion, Springer-Verlag Berlin Heidelberg 2003, 2006.

[6] A. S. Brown and M. A. Green, Impurity photovoltaic effect: Fundamental energy conversion efficiency limits, J. Appl. Phys., 92 (2002) 1329-1336.

[7] P. Baettig, C. Ederer and N.A. Spaldin, First principles study of the multiferroics $BiFeO_3$, Bi_2FeCrO_6, and $BiCrO_3$: Structure, polarization, and magnetic ordering temperature, Phys. Rev. B 72 (2005) 214105.

[8] R. Nechache, C. Harnagea, S. Licoccia, E. Traversa, A. Ruediger, A. Pignolet, and F. Rosei, Photovoltaic properties of Bi_2FeCrO_6 epitaxial thin films, Appl. Phys. Lett. 98 (2011) 202902.

[9] R. Nechache, C. Harnagea, S. Li, L. Cardenas, W. Huang, J. Chakrabartty and F. Rosei, Band-gap tuning of multiferroic oxide solar cells, Nat. Photonics 9 (2015) 61–67.

[10] R. Seshadri, N.A. Hill, Visualizing the Role of Bi 6s "Lone Pairs" in the Off-Center Distortion in Ferromagnetic $BiMnO_3$, Chem. Mater. 13 (2001) 2892.

[11] J. B. Neaton, C. Ederer, U. V. Waghmare, N. A. Spaldin, and K. M. Rabe, First-principles study of spontaneous polarization in multiferroic $BiFeO_3$, Phys. Rev B 71 (2005) 014113.

[12] ASTM G173-03 Reference Spectra: http://rredc.nrel.gov/solar/spectra/am1.5/ASTMG173/ASTMG173.html

[13] V. M. Fridkin, Photoferroelectrics, Springer-Verlag Berlin Heidelberg New York 1979; M. E. Lines, Principles and applications of ferroelectrics and related materials, Oxford University Press, 1977; K. M. Rabe, C. H. Ahn, J-M Triscone, Physics of Ferroelectrics, Springer-Verlag Berlin Heidelberg 2007.

[14] F. Liu, W. Wang, L. Wang, and G. Yang, Ferroelectric-semiconductor photovoltaics: Non-PN junction solar cells, App. Phys. Lett. 104 (2014) 103907.

[15] W. Kohn and L. J. Sham, Self-Consistent Equations Including Exchange and Correlation Effects, Phys. Rev., 140 (1965) A1133-A1138.

[16] J. M. Soler, E. Artacho, J. D. Gale, A. García, J. Junquera, P. Ordejon, and D. Sánchez-Portal, The SIESTA Method for Ab initio Order-N Materials Simulation, J. Phys.: Condens. Matter, 14 (2002) 2745-2779, and references therein.

[17] V. I. Anisimov, J. Zaanen, and O. K. Andersen, Band Theory and Mott Insulators: Hubbard U instead of Stoner I, Phys. Rev. B, 44 (1991) 943-954; V. I. Anisimov, I. V. Solovyev, and M. A. Korotin, M. T. Czyyk, and G. A. Sawatzky, Density-Functional Theory and NiO Photoemission Spectra, Phys. Rev. B, 48 (1993) 16929–16934.

[18] C. Tablero, Representations of the Occupation Number Matrix on the LDA/GGA+U Method, J. Phys.: Condens. Matter, 20 (2008) 325205.

[19] C. Tablero, Effects of the Orbital Self-interaction in both Strongly and Weakly Correlated Systems, J. Chem. Phys., 130 (2009) 054903.

[20] D. D. O'Regan, M. C. Payne, and A. A. Mostofi, Subspace Representations in Ab initio Methods for Strongly Correlated Systems, Phys. Rev. B, 83 (2011) 245124.

[21] M. Grisolía, P. Rozier, and M. Benoit, Density Functional Theory Investigations of the Structural and Electronic Properties of Ag2V4O11, Phys. Rev. B, 83 (2011) 165111.

[22] J. P. Perdew, K. Burke, and M. Ernzerhof, Generalized Gradient Approximation Made Simple, Phys. Rev. Lett., 77 (1996)3865-3868.

[23] N. Troullier and J. L. Martins, Efficient Pseudopotentials for Plane-wave Calculations, Phys. Rev. B, 43 (1991) 1993-2003.

[24] L. Kleinman and D. M. Bylander, Efficacious Form for Model Pseudopotentials, Phys. Rev. Lett., 48 (1982) 1425-1428; D. M. Bylander and L. Kleinman, 4f Resonances with Norm-conserving Pseudopotentials, Phys. Rev. B, 41 (1990) 907-912.

[25] O. F. Sankey and D. J. Niklewski, Ab initio Multicenter Tight-binding Model for Molecular-dynamics Simulations and Other Applications in Covalent Systems, Phys. Rev. B, 40 (1989) 3979-3995.

[26] I.P.A. Bakar, M.H. Hassan, M.K. Yaakob, M.F.M. Taib1, A.M.M. Ali1, O.H. Hassan, M.S.M. Deni1, M.Z.A. Yahya, Self-interaction Correction in Density Functional Theory of Multiferroic Double Perovskite Bi_2FeCrO_6 Properties, *Int. J. Electroactive Mater.* 2 (2014) 40-45.

[27] S. Zhe-Wen and L. Bang-Gui, Electronic structure and magnetic and optical properties of double perovskite Bi_2FeCrO_6 from first-principles investigation, Chin. Phys. B Vol. 22 (2013) 047506.

[28] N. G. Park, Organometal Perovskite Light Absorbers Toward a 20% Efficiency Low-Cost Solid-State Mesoscopic Solar Cell, J. Phys. Chem. Lett., 4 (2013) 2423−2429.

[29] Editorial. Reporting Solar Cell Efficiencies in Solar Energy Materials and Solar Cells, Sol. Energy Mater. Sol. Cells 92 (2008) 371−373.

List of Figures

Figure 1: Absorption coefficient split into spin polarizations (+ and – for spin up and down respectively). The band gap energy E_g have been chosen as the energy origin.

Figure 2: More important absorption coefficients split into atomic angular momentum contributions $\alpha_{l_A l_B}^{AB}$ as function of the energy for (a) spin up and (b) spin down components. The band gap energy E_g have been chosen as the energy origin.

Figure 3: Efficiency η (%) as a function of the cell thickness *w* for the spin-up (+), spin-down (-) and total (t) under (a) AM1.5G and (b) BB illumination spectrum. The fine and thick lines correspond to light concentration factor f_c = 1 (without concentration) and maximum concentration (f_c =max~ 46200).

Figure 4: Maximum efficiency η (%) and output voltage (v) as a function of β (degree of removal of radiative recombination current).

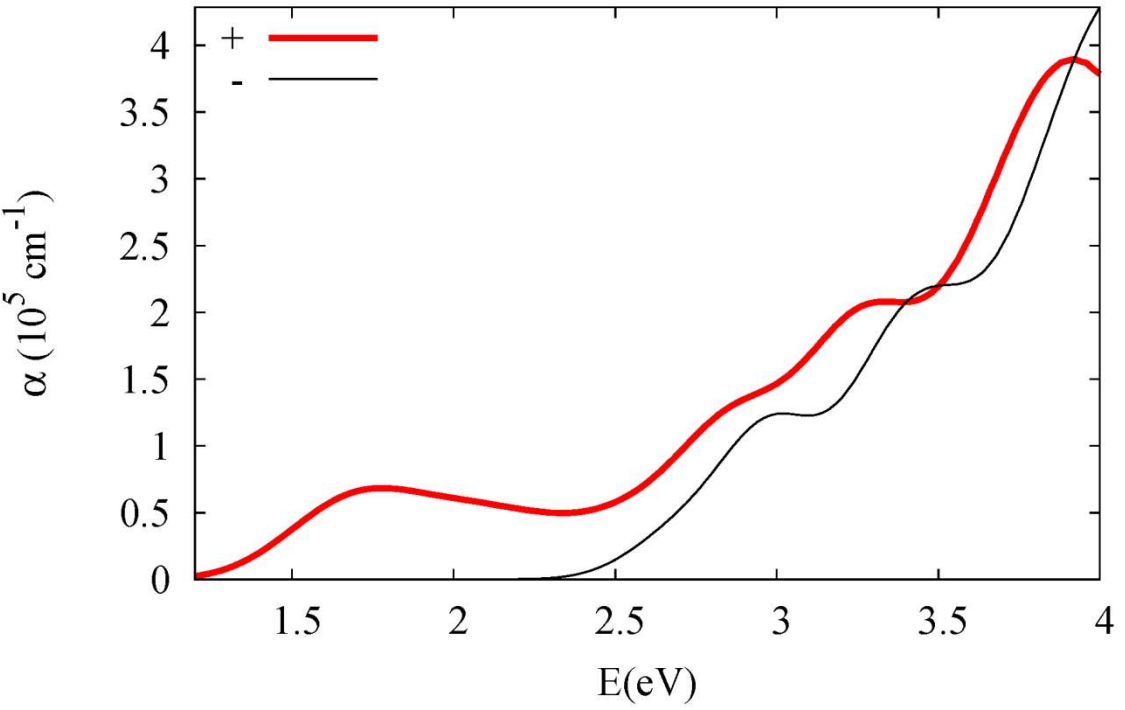

Figure 1

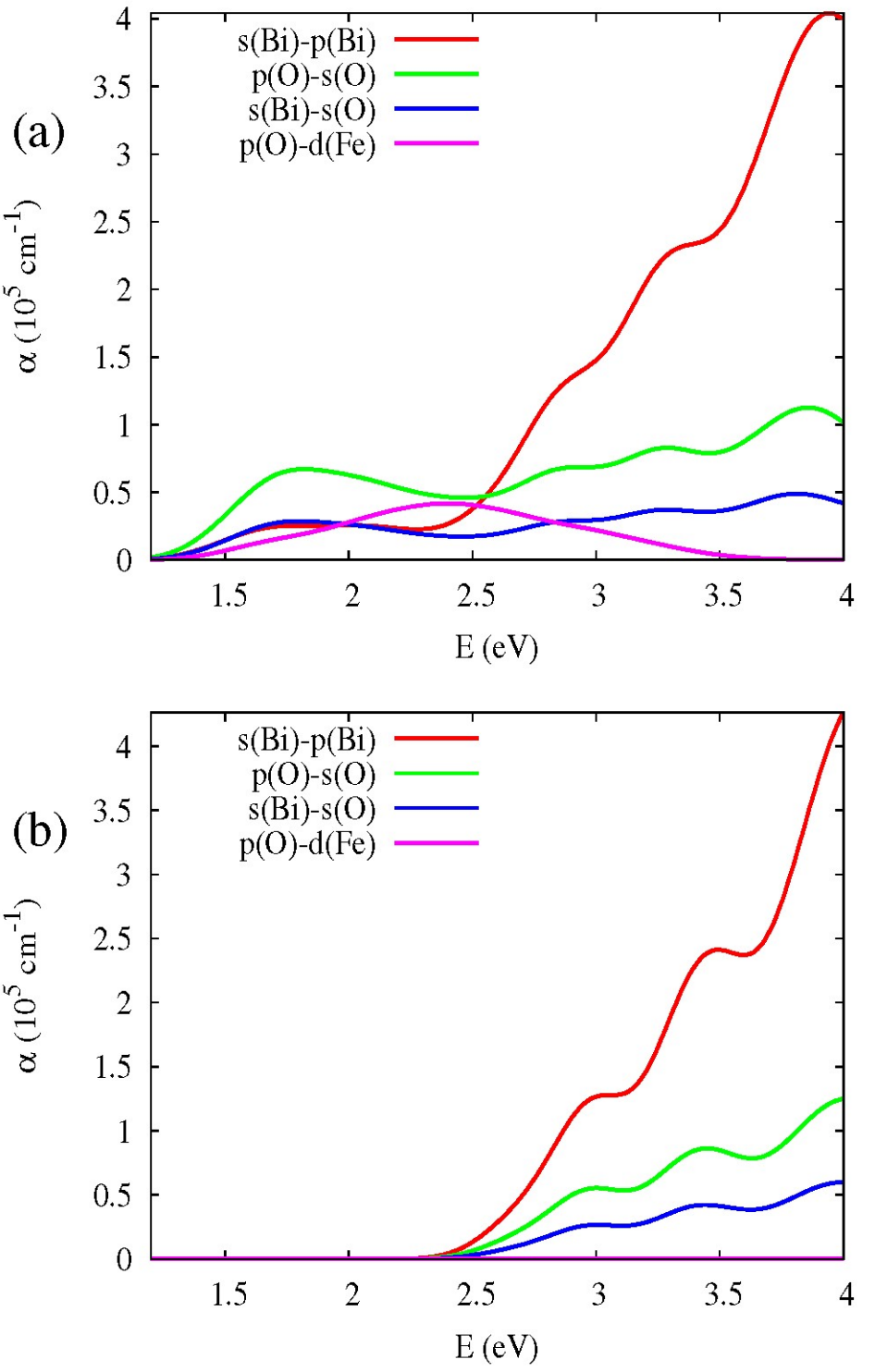
(a)
s(Bi)-p(Bi)
p(O)-s(O)
s(Bi)-s(O)
p(O)-d(Fe)
α (10^5 cm^-1)
E (eV)
(b)
s(Bi)-p(Bi)
p(O)-s(O)
s(Bi)-s(O)
p(O)-d(Fe)
α (10^5 cm^-1)
E (eV)

Figure 2

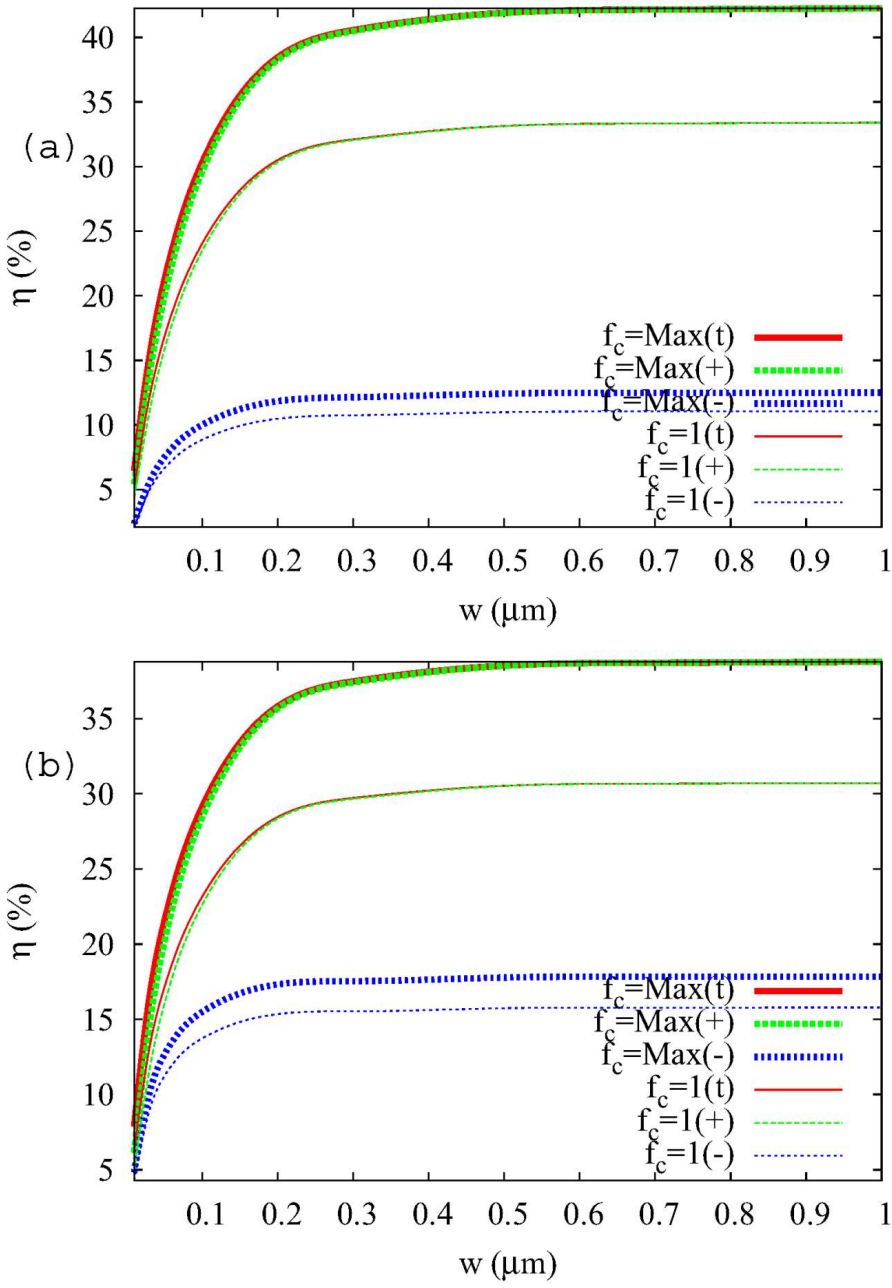
(a)
η (%)
w (μm)
f_c=Max(t)
f_c=Max(+)
f_c=Max(-)
f_c=1(t)
f_c=1(+)
f_c=1(-)
(b)
η (%)
w (μm)
f_c=Max(t)
f_c=Max(+)
f_c=Max(-)
f_c=1(t)
f_c=1(+)
f_c=1(-)

Figure 3

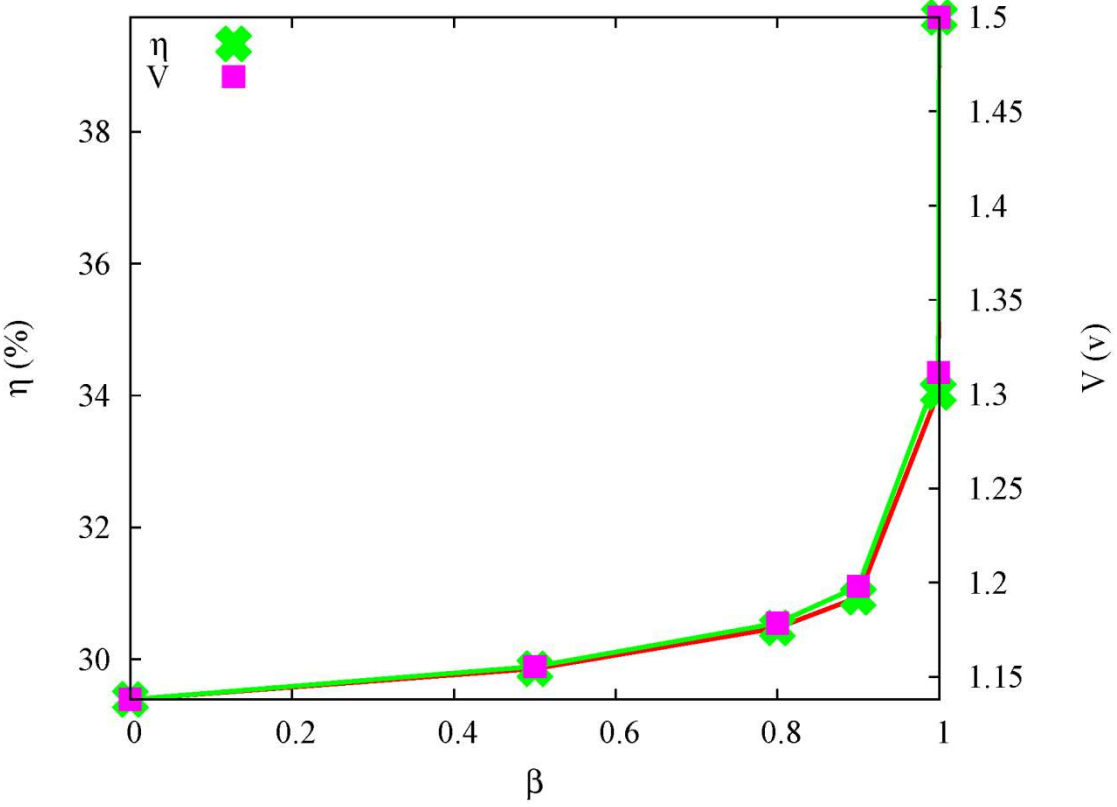

Figure 4